Initial Radiance Validation of the Microsized Microwave Atmospheric Satellite-2A

Citation: Crews, Angela et al. "Initial Radiance Validation of the Microsized Microwave Atmospheric Satellite-2A." IEEE Transactions on Geoscience and Remote Sensing 59, 4 (April 2021): 2703 - 2714. © 2021 IEEE

As Published: http://dx.doi.org/10.1109/tgrs.2020.3011200

Publisher: Institute of Electrical and Electronics Engineers (IEEE)

Persistent URL: https://hdl.handle.net/1721.1/130991

Version: Author's final manuscript: final author's manuscript post peer review, without publisher's formatting or copy editing

Initial Radiance Validation of the Micro-sized Microwave Atmospheric Satellite (MicroMAS-2A)

Angela Crews, William Blackwell, R. Vincent Leslie, Michael Grant, Idahosa Osaretin, Michael DiLiberto, Adam Milstein, Stephen Leroy, Amelia Gagnon, and Kerri Cahoy

***Abstract*—The Micro-Sized Microwave Atmospheric Satellite (MicroMAS-2A) is a 3U CubeSat that launched in January 2018 as a technology demonstration for future microwave sounding constellation missions, such as the NASA Time-Resolved Observations of Precipitation structure and storm Intensity with a Constellation of Smallsats (TROPICS) mission now in development. MicroMAS-2A has a miniaturized 1U 10-channel passive microwave radiometer with channels near 90, 118, 183, and 206 GHz for moisture and temperature profiling and precipitation imaging [4]. MicroMAS-2A provided the first CubeSat atmospheric vertical sounding data from orbit and to date is the only CubeSat to provide temperature and moisture sounding and surface imaging. In this paper, we analyze six segments of data collected from MicroMAS-2A in April 2018 and compare them to ERA5 reanalysis fields coupled with the Community Radiative Transfer Model (CRTM). This initial assessment of CubeSat radiometric accuracy shows biases relative to ERA5 with magnitudes ranging from 0.4 to 2.2 K (with standard deviations ranging from 0.7 to 1.2 K) for the four mid-tropospheric temperature channels and biases of 2.2 and 2.8 K (standard deviations 1.8 and 2.6 K) for the two lower tropospheric water vapor channels.**

***Index Terms*—Radiance validation, microwave radiometers, CubeSats, MicroMAS-2A**

I. Introduction

NANOSATELLITES are now proving themselves on orbit as viable weather forecasting platforms. The reduced cost and access to space compared with traditional satellites makes constellations more feasible. Constellations offer the advantage of increased observation density, expanded spatial coverage, and improved revisit time. In this work, we present results from initial radiance validation of MicroMAS-2A data using comparisons to ERA5 global reanalysis data [1] coupled with the Community Radiative Transfer Model (CRTM) [2].

MicroMAS-2A was a technology demonstration mission with objectives to verify key CubeSat components for a minimum of a three month period: 1) radiometer 2) scanner assembly and 3) bus. MicroMAS-2A met these objectives and provided the first CubeSat microwave atmospheric sounder data from orbit. However, only limited data segments were downlinked due to challenges communicating with the ground station and an anomaly with the on-board radio.

Using the relatively limited dataset available from MicroMAS-2A, this work suggests CubeSats with miniature microwave radiometers can achieve measurements that are useful for numerical weather prediction and other scientific applications after performing on-orbit calibration and validation. MicroMAS-2A aids to promote the idea that CubeSats have the potential to provide a weather monitoring platform at significantly reduced cost and lower revisit times than current platforms.

This paper is organized as follows. In Section 2, we provide background information on MicroMAS-2A. In Section 3, we describe our approach for on-orbit calibration corrections and radiance validation. On-orbit calibration corrections are derived by comparing the MicroMAS-2A datasets to datasets from the MicroWave Humidity Sounder (MWHS)-2, after which validation is performed by comparing the corrected MicroMAS-2A datasets to CRTM with ERA5 atmospheric inputs. Section 4 gives an overview of the data segments utilized for this initial analysis, and Section 5 details results for calibration and validation. A brief conclusion and discussion of future work is presented in Section 6.

II. Background

A. MicroMAS-2A

The Micro-Sized Microwave Atmospheric Satellite (MicroMAS-2A) is a 3U CubeSat with a miniaturized multi-band cross-track-scanning microwave radiometer that was launched on January 11, 2018. MicroMAS-2A is the successor to the previous CubeSat mission MicroMAS-1 that was deployed from the International Space Station (ISS) in 2015 [3]. MicroMAS-2A has an improved 10-channel radiometer, including a window channel at 89 GHz; temperature and precipitation observations near 118 GHz; humidity and precipitation observations near 183 GHz; and cloud ice observations near 206 GHz. The MicroMAS-2A Channel 10 (206 GHz) had EMI interference that made the channel unusable. The interference occurred within the shared housing of the Intermediate Frequency Processors (IFPs), and was

This paper was submitted 4 June 2019 for review. This work was supported by a NASA Space Technology Research Fellowship NNX16AM73H.

A. Crews, A. Gagnon, and K. Cahoy are with Massachusetts Institute of Technology, Cambridge MA 02139 USA (email: crewsab@mit.edu, agagnon@mit.edu, kcahoy@mit.edu).

W. Blackwell, R. Leslie, I. Osaretin, M. DiLiberto, and A. Milstein are with MIT Lincoln Laboratory, Lexington MA 02421 USA (email: wjb@ll.mit.edu, lesliev@ll.mit.edu, idahosa.osaretin@ll.mit.edu, mike.diliberto@ll.mit.edu, milstein@ll.mit.edu).

M. Grant is with NASA Langley, Hampton VA 23666 USA (email: michael.s.grant@nasa.gov).

S. Leroy is with Atmospheric and Environmental Research, Inc., 131 Hartwell Ave., Lexington, MA 02421 USA (email: sleroy@aer.com).

remedied in TROPICS by using a direct-detect receiver architecture for the G-band channels (i.e., no G-band intermediate frequencies). Due to the interference, Channel 10 is not included in this analysis.

MicroMAS-2A is a technology demonstration for future missions such as the CubeSat constellation TROPICS, a NASA Earth Venture-Instrument (EVI)-3 selected mission of six 3U CubeSats that is scheduled for launch no earlier than 2021 [4]. Seven TROPICS flight payloads have been built and tested, and thermal vacuum calibration results indicate substantially improved noise performance and absolute calibration accuracy and stability relative to MicroMAS-2A [5]. Table 1 provides a comparison between the MicroMAS and TROPICS CubeSats.

Table 1: Comparison between MicroMAS and TROPICS CubeSat missions [6]

CubeSat Mission	Details
MicroMAS-1	Launched July 2014 and deployed from ISS in 2015 [3] Measure 3D temperature Single band at 108-118 GHz (9 channels) Three contacts before communications failed
MicroMAS-2A	Launched Jan 2018 Measure 3D temperature, 3D water vapor, and cloud ice 4 bands at 89 GHz, 118 GHz, 183 GHz, and 206 GHz (10 channels) 2A provided first CubeSat microwave atmospheric sounder data from orbit (this work)
TROPICS	Launch no earlier than 2021 Measure 3D temperature, 3D water vapor, and cloud ice 4 bands at 92 GHz, 118 GHz, 183 GHz, and 205 GHz (12 channels) Constellation of six CubeSats in three orbital planes

The MicroMAS-2A CubeSat has a 1.5 U Pumpkin, Inc. bus, a 0.5 U Attitude Determination and Control (ADCS) unit, and a 1.0 U passive microwave radiometer payload. MicroMAS-2 is a dual-spinner; the ADCS maintains a 3-axis stabilized orientation while the payload is rotated at 30 rpm. The dual spinner configuration allows the radiometer's field of view to sweep perpendicularly to the satellite ground track, enabling a cross-track scan like typical larger microwave radiometer instruments while also permitting a full 360-degree field of view that is very useful for calibration using cosmic background radiation and celestial sources. MicroMAS-2A was launched as a secondary payload on the Polar Satellite Launch Vehicle (PSLV) into a 500-km sun-synchronous orbit with an inclination of 97.55°. Fig. 1 shows an image of the as-built MicroMAS-2A.

Fig. 1. The MicroMAS-2A satellite is 4.5 kg and 34 x 10 x 10 $cm^{3.}$ [MIT LL]

B. Miniaturization of microwave radiometers

Miniaturized microwave radiometers are particularly well-suited for CubeSats, given technological advances that enable frequency multiplexing techniques to be accomplished in a compact form factor [7]. Other elements of microwave radiometer missions such as their relatively large ground footprints, modest pointing requirements, and relatively low data rates make them suitable for CubeSat missions [8].

However, miniaturization comes with challenges related to calibration. Space-borne microwave radiometers typically use a two-point calibration scheme, with deep space used as the "cold" measurement and blackbody calibration targets used as the "warm" measurements. Traditional blackbody calibration targets are too bulky to be easily used on 3U CubeSats without performance degrading sacrifices to the amount of shrouding and/or aperture size. In contrast, noise diodes used for the "warm" calibration point are much smaller. For example, the noise diodes flown on the MicroMAS missions are on the order of a few mm^2 in size [9]. Noise diodes have been flown on previous missions such as JASON-1, where the noise diodes were shown to have a long term drift over a four year time period in the range of 0.2-3.0% [10].

The more recent Global Precipitation Measurement (GPM) mission used both noise diodes and blackbody calibration targets for calibration of the GPM Microwave Imager (GMI). Five of the six noise diodes on GMI were extremely stable, with a drift of less than 0.1K over the four years following on-orbit calibration and validation [11]. In fact, the GMI mission has used the noise diodes to correct for thermal gradients in the blackbody calibration targets [12]. The MicroMAS and TROPICS CubeSats use similar noise diode technology as GMI for the W/F-band system. However, the GMI noise diodes have only been previously demonstrated on-orbit up to 40 GHz. Prelaunch noise diode testing for the TROPICS CubeSat constellation mission has included an extensive screening of noise diode stability, as recommended in [12].

In order to ensure that CubeSat microwave radiometers such as MicroMAS-2A provide well-calibrated data, we develop

calibration and validation techniques to characterize the noise diode drift at MicroMAS/TROPICS frequencies of up to 183 GHz. In this work, we describe radiance validation techniques for MicroMAS-2A and assess its radiometric accuracy.

III. Description of the Data Used in this Study

A. Data Segment Overview

For the following analyses, we use six data segments that we refer to as **Segment 1** - **Segment 6**. Data Segments 1 & 2 are approximately 5 minutes long and are geolocated in a northern polar region near Alaska, while Data Segment 3 is located near Madagascar. Data Segment 4 is located off the coast of Australia, Data Segment 5 is located near the Red Sea, and Data Segment 6 is located in a swath from Alaska to Hawaii.

All six segments of data were taken on April 6, 2018, at the following times: Segment 1 05:17-05:22Z, Segment 2 02:12-02:17Z, Segment 3 05:46-05:55Z, Segment 4 02:16-02:23Z, Segment 5 07:13-07:22Z, and Segment 6 08:14-08:22Z. Fig. 2 shows a global plot of the six data segment images. The images show post-calibration brightness temperatures as measured by Channel 1 (89.0 GHz).

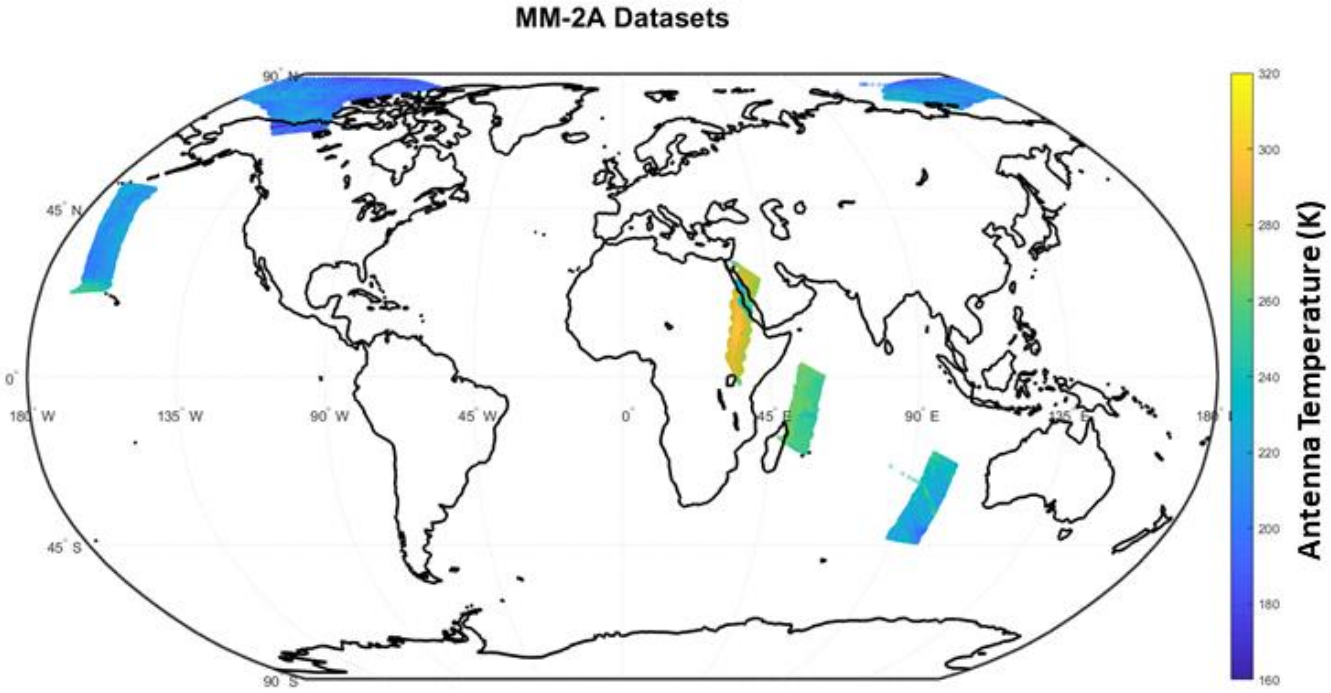

Fig. 2: Global map depicting the six MicroMAS-2A data segments used for this analysis. In this plot, we show the post-calibrated brightness temperatures measured by Channel 1 (89.0 GHz).

B. Geolocation Process and Timing Errors

The instrument data samples were geolocated by computing the Earth-fixed coordinates of intersection between the instrument line of sight vector and the Earth ellipsoid. This process requires the estimated spacecraft position, the estimated spacecraft attitude, the scan angle of the payload scanner, and the boresight angles of the instrument channels relative to the scanner block origin. The spacecraft position was computed using SGP4 propagation with the most recent available two-line element (TLE). The spacecraft attitude estimate was computed offline by playing back spacecraft telemetry through a slightly modified version of the flight software algorithms running onboard the spacecraft.

The flight algorithms compute an attitude estimate from the best available onboard attitude estimation sensors, including magnetometer, IR Earth horizon sensors (EHS), and coarse sun sensors (CSS). The estimate is then propagated using the angular rate measurements from the Inertial Measurement Unit (IMU). The algorithms employed on MicroMAS-2A are similar to those described by Quadrino [13], with a notable update: the Kalman filter described in [14] was used in place of the TRIAD algorithm to generate attitude estimates that are subsequently filtered as in [13]. Due to daytime anomalies in the magnetometer readings (apparently caused by panel currents) the magnetometer was not used for on-orbit attitude estimation.

Geolocation errors for the MicroMAS-2A data samples are determined based on pre-launch dynamic simulations and sensor models. Noise and systematic error sources (such as Earth solar reflections) are taken into the account. Our modeling shows that roll/pitch errors are approximately 1 degree each (with narrow EHS lock), while yaw errors are approximately 10 degrees. Yaw errors are significantly worse than roll/pitch errors due to anomalies in the magnetometer data, which caused a reliance on CSS. With these roll/pitch/yaw error assumptions, we estimate that geolocation error varies

from 12.3 km RMS near nadir up to 79.3 km RMS error at 42 degrees scan angle, as shown in Figure 3.

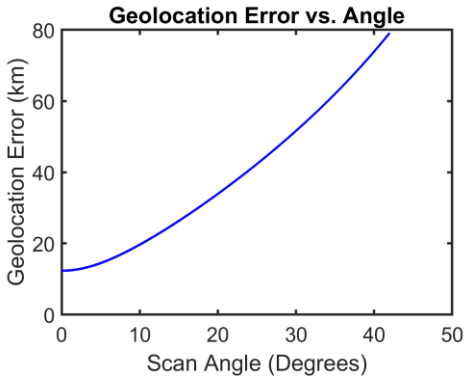

Fig. 3: The MicroMAS-2A geolocation error is estimated to range from 12.3 km RMS at nadir to 79.3 km RMS at 42° scan angle.

The timing of the spacecraft attitude telemetry was synchronized to UTC using a time probe command uplinked to the spacecraft from the ground station. The timestamps of the payload samples relative to UTC were fine-tuned during geolocation ground processing by correcting for a slight along-track shift in the observed Alaska ground crossings. The instrument channel boresight angles, relative to the scanner block, were measured prior to launch.

Timing errors are slowly varying and contribute much smaller amounts of geolocation errors than the ADCS sensors themselves. With static timing offsets removed by our coastal matching technique, timing errors for the MicroMAS-2A datasets are assessed to be no greater than 1 second.

IV. Approach

In this section we describe our approach to radiance validation using ERA5/CRTM and calibration using MWHS-2. We begin by describing the radiative transfer model used in our validation method.

A. Radiance Validation

Radiance validation estimates the *quality* (e.g. bias and standard deviation) of a data product when compared to other sources. Radiative transfer models with atmospheric inputs from sources such as GPS Radio Occultation (GPSRO), radiosondes, and Numerical Weather Prediction (NWP) models are used to simulate expected brightness temperatures for comparison to the sensor data. Simulated brightness temperatures are then compared to actual satellite brightness temperatures in order to determine radiometric accuracy.

Line-by-line (LBL) radiative transfer models (RTM's) calculate absorption and transmittance at individual spectral lines. However, these models are computationally expensive and can take up to an hour to calculate brightness temperature for a single channel [15]. So-called *fast* radiative transfer models have been developed to speed up calculations by using look-up tables and parameterizing absorption and scattering. Fast models provide a statistical fit to LBL models, and often take on the order of a millisecond to compute a single channel [15]. For this research, we use the fast Joint Center for Satellite Data Assimilation (JCSDA)-developed Community Radiative Transfer Model (CRTM) [2], with MicroMAS-2A measured channel Spectral Response Functions (SRFs).

CRTM requires atmospheric profiles, surface information, and satellite characteristics. Surface information that is input into CRTM includes the surface type, land fraction, surface winds, and sea surface temperature (SST) or land surface temperature (LST). We use a value of 0.92 for ice emissivity. Water emissivity is calculated using FASTEM6 in CRTM [16,17]. We utilize surface information from the ERA5 European Centre for Medium-Range Weather Forecasts (ECMWF) reanalysis dataset [1], as no Constellation Observing System for Meteorology, Ionosphere and Climate (COSMIC) Global Positioning System (GPS) Radio Occultation (GPSRO) atmospheric profiles [18] or Global Climate Observing System (GCOS) Reference Upper-Air Network (GRUAN) radiosonde station atmospheric profiles [19] exist within our time and distance filters (<1 hour, <50 km) for the MicroMAS-2A data segments.

ERA5 is a publicly available reanalysis dataset from ECMWF that creates global estimates by combining historical observations with modeling and data assimilation systems [1]. ERA5 has a spatial resolution of 31 km and a temporal resolution of one hour. Estimates every hour are made possible through the use of a 4D-var assimilation model, which incorporates exact timing of observations into the model [20].

B. Sensor Comparisons

The MicroWave Humidity Sounder-2 (MWHS-2) is a four band, 15-channel cross-track microwave sounder on the China Meteorological Administration (CMA)'s Feng Yun (FY)-3C polar orbiting weather satellite. MWHS-2 is the first space-borne nadir sounder instrument to have sounding channels centered around the 118.75 GHz oxygen line [21]. MWHS-2 has a specified calibration accuracy better than 2.0 K for all channels [22]. In this work, MWHS-2 data are used to derive a single calibration parameter (for each MicroMAS-2A channel) in a very simple (constant offset) calibration model that was derived during prelaunch TVAC testing. Table 2 provides a comparison of the frequencies and passbands of the MicroMAS-2A and MWHS-2 channels. Table 2 also indicates which MWHS-2 channels are most closely matched in frequency to MicroMAS-2A channels. In addition to channel frequency, we consider the instrument weighting function peaks in order to provide a comparison of how closely the channels match each other. Weighting functions show the change of total transmittance with respect to pressure, and demonstrate the sensitivity of channels at different altitudes in the atmosphere. By comparing the weighting function peaks of instruments with somewhat dissimilar channel frequencies, we can determine reasonable channel matches for comparisons.

As shown in the weighting function plots in Fig. 4, MicroMAS-2A Channels 1, 7, 8, and 9 have nearly identical matches to MWHS-2 Channels 1, 11, 13, and 15. MicroMAS-2A Channels 2-6 are most closely matched to MWHS-2 Channels 7, 6, 5, and 2. From Fig. 4, the matchups for

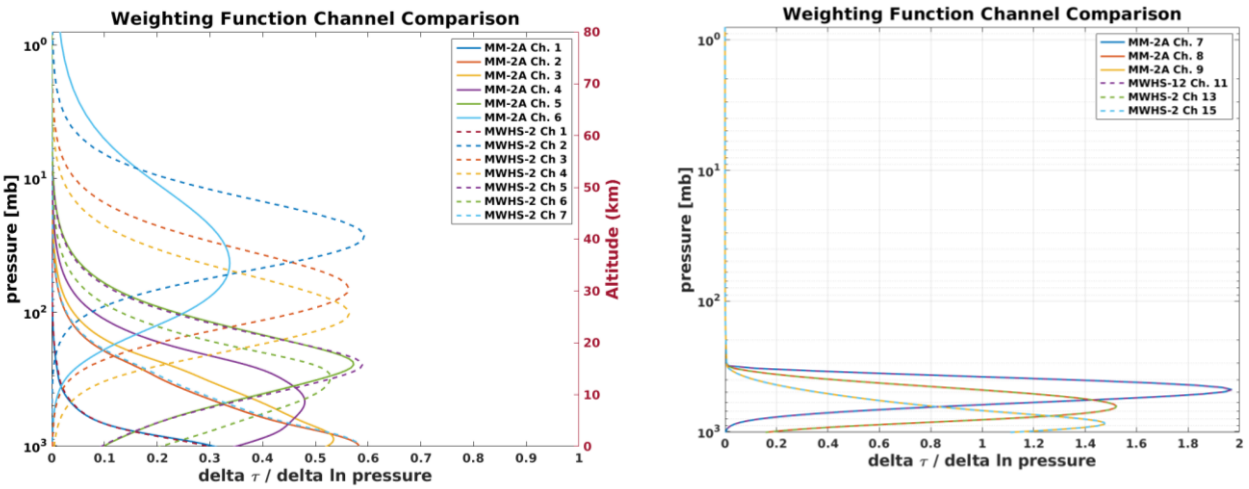

Fig. 4: Weighting function comparison of channels between MicroMAS-2A and MWHS-2, plotted by normalized change in transmittance per pressure level. For these plots, we have assumed boxcar SRFs for both sensors.

Table 2: Channel Comparison between MicroMAS-2A and MWHS-2. Weighting function peaks are compared using boxcar approximated Spectral Response Functions (SRFs).

MicroMAS-2A		MWHS-2	
RF Center Freq/ Bandwidth	**WF peak** (hPa/ delta τ/delta ln px)	**RF Center Freq/ Bandwidth**	**WF peak** (hPa/ delta τ/delta ln px)
Ch 1: 93.6; 1.0 GHz	986.1 hPa; 0.30	Ch 1: 89 1.5 GHz	986.1 hPa; 0.28
Ch 2: 116.16; 0.48 GHz	986.1 hPa; 0.58	Ch 7: 118.75 +/- 2.5; 0.2 GHz	986.1 hPa; 0.58
Ch 3: 116.68; 0.4 GHz	891.75 hPa; 0.53	Ch 7: 118.75 +/- 2.5; 0.2 GHz	986.1 hPa; 0.58
Ch 4: 117.29; 0.46 GHz	459.7 hPa; 0.50	Ch 6: 118.75 +/- 1.1; 0.2 GHz	314.1 hPa; 0.53
Ch 5: 117.95; 0.48 GHz	247.4 hPa; 0.57	Ch 5: 118.75 +/- 0.8; 0.2 GHz	247.4 hPa; 0.59
Ch 6: 118.64; 0.42 GHz	43.1 hPa; 0.34	Ch 2: 118.75 +/- 0.08; 0.02 GHz	26.18 hPa; 0.59
Ch 7: 183.312 +/- 1; 0.5 GHz	478 hPa; 1.97	Ch 11: 183.31 +/- 1; 0.5 GHz	478 hPa; 1.97
Ch 8: 183.312 +/- 3; 1.0 GHz	639.1 hPa; 1.52	Ch 13: 183.31 +/- 3; 1.0 GHz	639.1 hPa; 1.52
Ch 9: 183.312 +/- 7; 2.0 GHz	898.6 hPa; 1.476	Ch 15: 183.31 +/- 7; 2.0 GHz	878.6 hPa 1.476

MicroMAS-2A Channels 4 and 6 are seen to be the least accurate.

C. Spectral Response Functions

The weighting functions described in Table 2 (WF peaks) and Fig. 4 assume a boxcar approximation for the Spectral Response Function (SRF) of all sensor channels. However, our analysis shows that the boxcar approximation is not accurate enough to model MicroMAS-2 channels, particularly for the F-band channels. Fig. 5 shows the MicroMAS-2A SRFs for both G-band and F-band. For the G-band channels, the boxcar approximation (depicted in the dashed lines) closely approximates the as-measured SRFs. However, the as-measured F-band SRFs show frequency contributions outside of the desired bandwidth. Because MicroMAS-2A was a technology demonstration with a limited schedule and budget, the F-band channels were not optimized prior to launch. It should be noted that a different Intermediate Frequency (IF) filter design for the TROPICS CubeSats has substantiallyimproved the as-measured F-band SRF passband shapes, resulting in near-negligible out-of-band responses for these channels.

To determine the impact of boxcar approximations, we

.

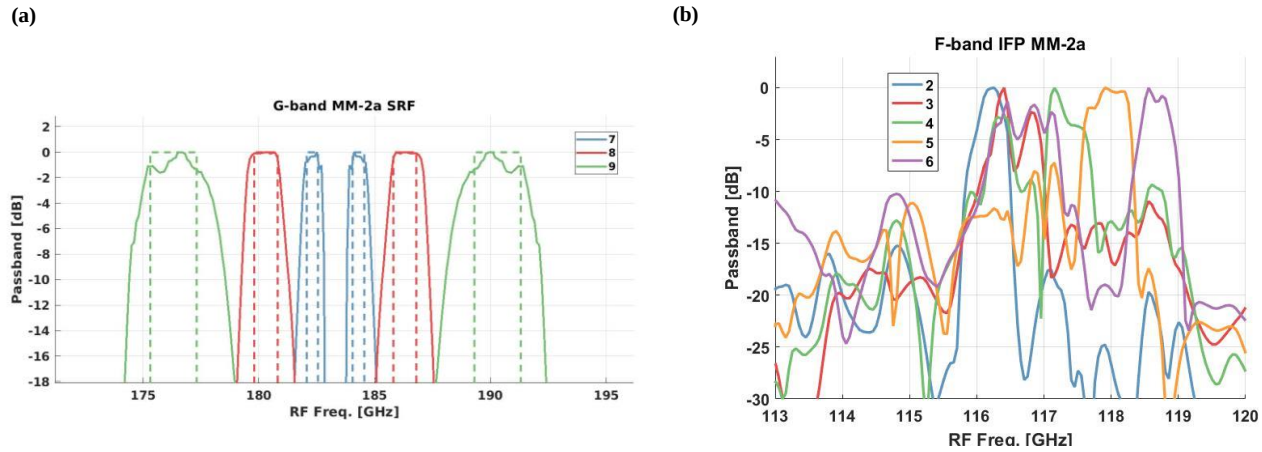

Fig.5: As-measured MicroMAS-2A SRF. 4(a) shows the MicroMAS-2A G-band Channels 7-9. The boxcar approximation (dashed lines) is a good comparison to the actual SRF (solid). 4(b) shows the MicroMAS-2A F-band Channels 2-6. Due to MicroMAS-2A being a technology demonstration with a limited schedule and budget, the SRFs were not optimized prior to launch. Contributions from frequencies are seen outside of their desired bandwidths.

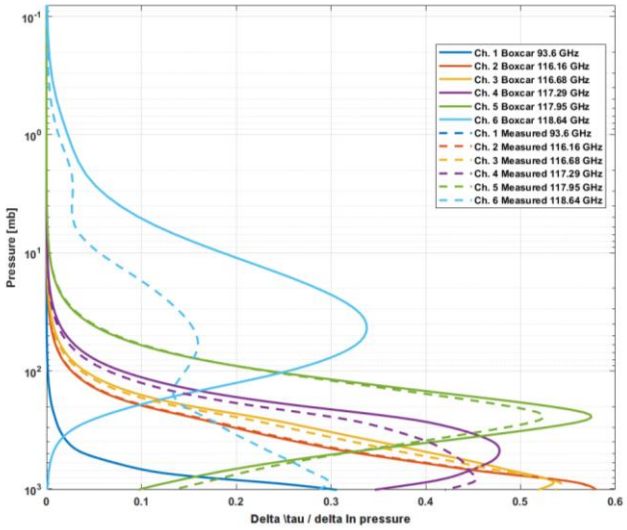

Fig. 6: MicroMAS-2A weighting functions for boxcar (solid) and as-measured SRF. Dashed lines depict as-measured SRF.

plotted the MicroMAS-2A weighting functions for both boxcar and as-measured SRFs, as shown in Fig. 6. The boxcar SRF is plotted with the solid line, while the as-measured SRF is plotted with the dashed line. It can be seen that Channel 6 has extra peaks in its weighting function, which correlates to the out of band frequency measurements in F-band shown in Fig. 5. Channel 4 also shows a significantly different weighting function peak for boxcar versus as-measured SRF. Using the as-measured SRF weighting functions for MicroMAS-2A, we average multiple channels from MWHS-2 in order to approximate the MicroMAS-2A channel weighting functions. The resulting F-band channel comparisons for MicroMAS-2A Channels 2-6 are shown in Table 3.

In order to quantify the effect of weighting function disparities between MicroMAS-2A

Table 3: F-band channel weighting functions comparison between MicroMAS-2A and MWHS-2.

MicroMAS-2A WF Peaks (hPa/ delta τ/delta ln px)	**MWHS-2 WF Peaks** (hPa/delta τ/delta ln px)
Ch 2: 986.1 hPa/0.5818	Ch 7: 986.1 hPa/0.5829
Ch 3: 891.8 hPa/0.5343	Ch 7: 986.1 hPa/0.5829
Ch 4: 802.4 hPa/0.4534	Ch 6 & 7: 650.1 hPa/0.5557
Ch 5: 247.4 hPa/0.5727	Ch 5: 247.4 hPa/0.5725
Ch 6: 852.8 hPa/0.2972 and 56.13 hPa/0.1597	Ch 6 & 7: 650.1 hPa/0.5557; Ch 3: 66.1 hPa/0.5632

and MWHS-2, we analyze brightness temperatures differences for our channel matchups using CRTM with NOAA-88b profiles. The NOAA-88b dataset is global and includes 7547 total clear sky radiosonde samples. CRTM is used to simulate channel brightness temperatures for each profile using MicroMAS-2A sensor characteristics (as-measured SRF) and MWHS-2 sensor characteristics (boxcar SRF). The simulated MicroMAS-2A minus MWHS-2 channel differences (i.e. MicroMAS-2A 'errors' with respect to MWHS-2) were averaged for all 7547 profile runs.

Results from the simulated instrument comparison, by channel matchups, are given in Table 4. Figure 7 is an example of a comparison between brightness temperature histograms: 1) actual radiances from all six segments (majority ocean surface) and 2) simulated ocean radiances from the global all-year clear-sky NOAA88b ensemble. In this example from MicroMAS-2A Channel 2, the actual MicroMAS-2A histogram has a similar

shape as the actual MWHS-2 histogram, but has a brightness temperature offset that is not seen in the simulated data. This is a clear example that a calibration correction to the noise diode temperature will move the actual histograms closer (see Section IV D).

Table 4: Mean difference and standard deviations between MicroMAS-2A and MWHS-2 using CTRM with NOAA-88b atmospheric profiles.

MM-2A Channel	MWHS-2 Channel	Mean Difference Error (K)	Mean Difference StdDev (K)
Ch 1	Ch 1	2.25 K	1.24 K
Ch 2	Ch 7	-0.18 K	0.11 K
Ch 3	Ch 7	-0.80 K	1.14 K
Ch 4	Ch 6 & 7	2.95 K	0.38 K
Ch 5	Ch 5	1.51 K	0.19 K
Ch 6	Ch 6 & 7, Ch 3	8.94 K	2.31 K
Ch 7	Ch 11	0.08 K	0.11 K
Ch 8	Ch 13	0.38 K	0.12 K
Ch 9	Ch 15	0.17 K	0.10 K

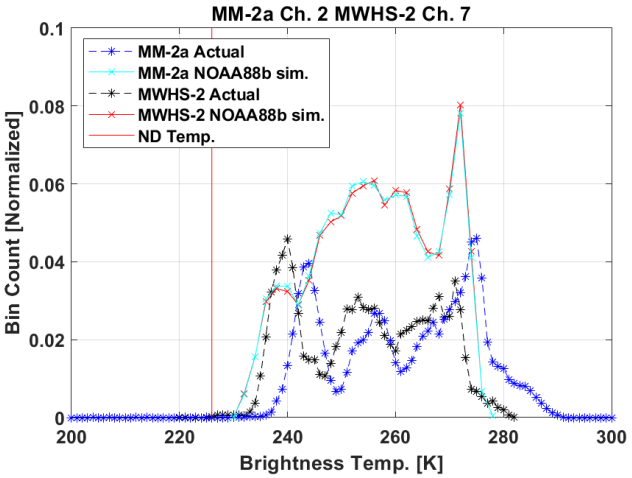

Figure 7: Brightness temperature histogram comparisons between actual MM-2a, actual MWHS-2, simulated MM-2a, and simulated MWHS-2. Actual data includes all six segments and simulated is the global clear sky NOAA88b dataset with simulated ocean surface. Red line is the MM-2a noise diode output at room temperature.

Channel 6 shows a mean error of 8.94 K. This error is attributed to the difficulty in matching the MWHS-2 channel weighting functions to the multiple peaks in the MicroMAS-2A Channel 6 as-measured SRF. Given the relatively large difference between the MicroMAS-2A Channel 6 and corresponding MWHS-2 channel matchup, we expect the validation errors for this channel to be large. The NOAA-88b MicroMAS-2A/MWHS-2 matchups for Channels 7-9 show the lowest mean errors (< 0.4 K). This is clearly due to the closely matched weighting function peaks and shapes for these channel matchups.

NOAA88b simulation analysis of the other channels indicated either a minor impact on the calibration correction or an overcompensation that will only increase the validation error in Section V B. We did not want to include simulation errors into the calibration correction since simulations were also used in the validation results, therefore the validation error will include some error from spectral mismatch in the calibration factors. Analysis from the spectral mismatch shows the mismatch will not artificially improve the validation results.

D. Calibration Correction Approach

After determining the best available channel pairings for comparison, we use MWHS-2 to determine on-orbit calibration corrections for MicroMAS-2A. Stray radiation during pre-launch thermal vacuum (TVAC) testing resulted in the data not being usable (except for non-linearity corrections), which necessitated the use of on-orbit techniques. In order to minimize atmospheric scene differences, the MWHS-2 datasets are chosen as close as possible in time (within +/- 95 minutes) to the MicroMAS-2A datasets and the images are masked and cropped to match the location of the MicroMAS-2A dataset images. Despite the best efforts to choose overlapping datasets in space and time, it is likely that the two instruments may still not be seeing the same thing in all channels that are being compared. The datasets between the two sensors have differing view angles; however, we assume that the histogram distribution of brightness temperatures for each data segment is similar for both instruments. A summary of the time and zenith angles for the MicroMAS-2A and matching MWHS-2 data segments is shown in Table 5. The dataset differences in Table 5 likely contribute to the differences in measured brightness temperatures.

On-orbit correction factors are derived using vicarious calibration [24]. We find correction factors by using a statistical comparison of histograms of measured brightness temperature between MicroMAS-2A and MWHS-2. The histogram comparisons, or matchups, yield corrections to the MicroMAS-2A noise diode temperature that are then incorporated into the calibration. Although noise diodes typically vary over instrument temperature, only limited noise diode temperature stability plots were available from MicroMAS-2A ground testing in the thermal vacuum chamber. We therefore assume a constant noise diode output with physical temperature for this study. However, a more representative linear-with-temperature noise diode transfer function will be investigated during future work which could further improve the results presented below.

In order to complete the histogram matchups, the MicroMAS-2A brightness temperature measured over a given data segment is used to generate a histogram, which is compared to the corresponding MWHS-2 brightness temperature histogram at the matching channel (see Table 2 and Table 3). We assume that the histogram distribution of

Table 5: Comparison of MicroMAS-2A and MWHS-2 data segment time and zenith angles. All data segments are from 6 Apr 2018.

Data Segment	MM-2A Time	MWHS-2 Time	MM-2A Zenith Angle	MWHS-2 Zenith Angle
1	0512-0522Z	0643-0647Z	-38 to +38 deg	-56 to -12.5 deg
2	0211-0221Z	0323-0328Z	-38 to +38 deg	-45 to +15 deg
3	0542-0552Z	0532-0539Z	-38 to +38 deg	-62 to +15 deg
4	0242-0249Z	0216-0223Z	-38 to +38 deg	-60 to -19 deg
5	0713-0722Z	0707-1915Z	-38 to +38 deg	-60 to -30 deg
6	0814-0822Z	0812-0821Z	-38 to +38 deg	0 to +50 deg

brightness temperatures for the scene is similar for both instruments. Both histograms are generated with 200 bins from 200 to 300 K and normalized such that the sum of the bar heights is equal to one. This normalization allows a more accurate histogram comparison between segments with differing number of total points. We then sweep through adjustments to the noise diode temperature until we find the noise diode temperature value corresponding to the minimum root sum square (RSS) of histogram bin differences.

An example is shown for MicroMAS-2A Channel 7, which is compared to MWHS-2 Channel 11 for Segment 1. In Fig. 8(a), the histogram of brightness temperatures is compared prior to the calibration correction. The MicroMAS-2A histogram is shown shifted to the left from the MWHS-2 histogram. We then adjust the single calibration parameter (noise diode temperature) for Channel 7 until the MicroMAS-2A histogram curve matches the MWHS-2 histogram curve, as shown in Fig. 8(b). The corresponding antenna temperature images for the Fig. 8 histograms are shown in Fig. 9. Fig. 9(a) shows the MicroMAS-2A image prior to the calibration correction, Fig. 9(b) shows the MicroMAS-2A image after the calibration correction, and Fig. 9(c) shows the corresponding MWHS-2 image. It can be seen that the MicroMAS-2A image features match the MWHS-2 image in scale after the calibration correction.

F. Selection of Points for Single Differences

MicroMAS-2A points for validation are selected from each segment that are >160 km apart, which ensures that each point analyzed is in a different 1° grid and uses a different ERA5 profile for simulation. The most accurate radiometric biases are developed by using profiles that take place in clear sky and over water; varying surface emissivity causes less accurate simulated brightness temperatures over land, and clouds affect the brightness temperature of sounding channels. Thus, all points are screened for over water and clear sky. Clear sky is determined by using cloud masks obtained from VIIR on FY-3C. Absolute scan angle is limited to less than 15 degrees.

Eight points from Segment 1, two points from Segment 2, twelve points from Segment 3, eight points from Segment 4, three points from Segment 5, and 11 points from Segment 6 passed our filters, which gives 41 total points to use for validation with CRTM/ERA5. After these points are selected, we find the atmospheric profiles correlating to each point from ERA5. These atmospheric profiles are then input to CRTM in order to simulate brightness temperatures for validation.

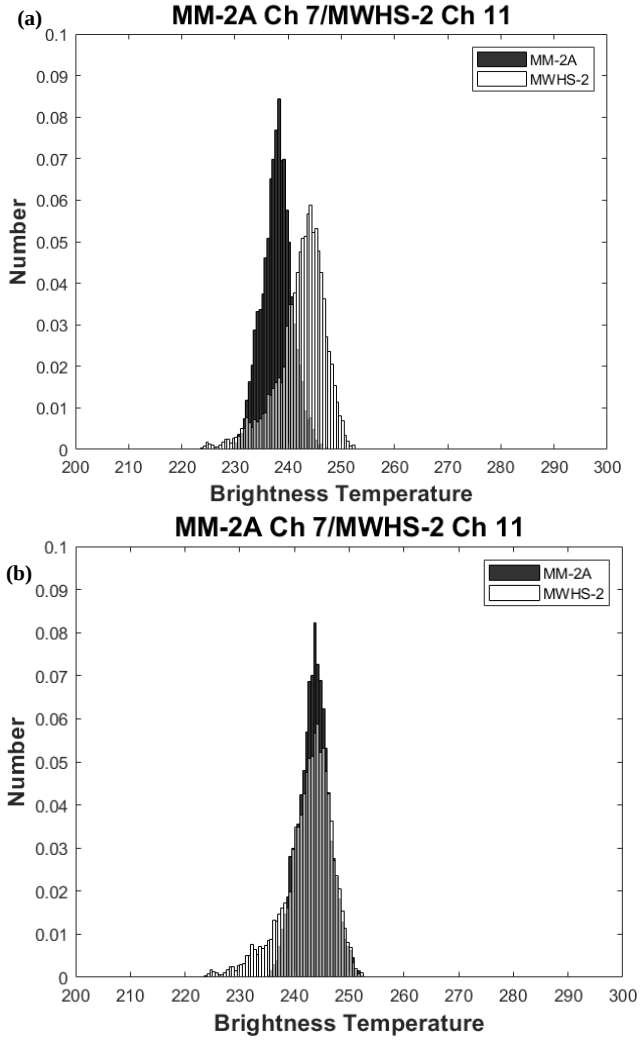

Fig.8: Histogram matchup between MicroMAS-2A and MWHS-2 for data segment 1 before the noise diode correction (a) and after the noise diode correction (b).

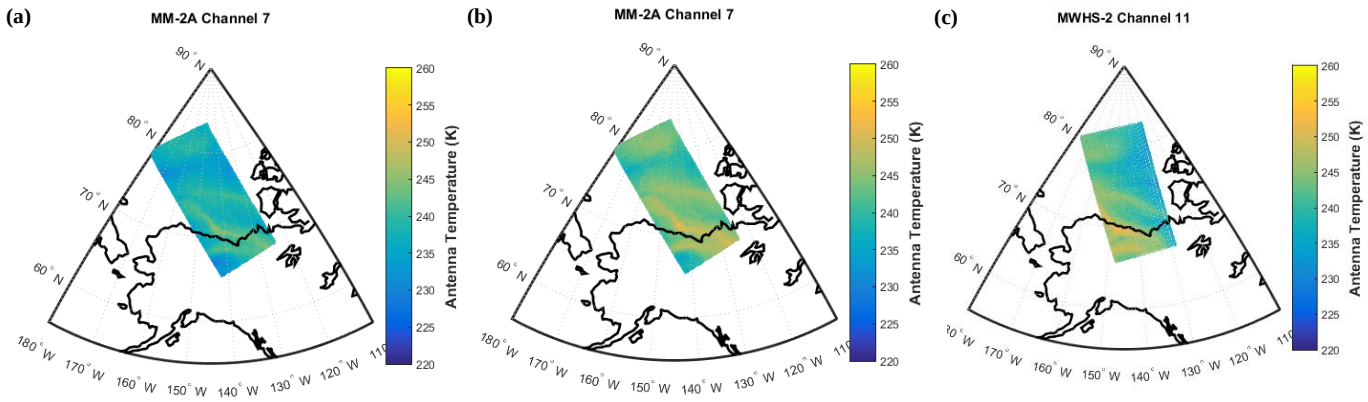

Fig.9: The MicroMAS-2A image for Data Segment 1 is compared to an MWHS-2 image (c) before the calibration correction (a) and after the calibration correction (b). After correction, the brightness temperature of the features in the images align.

Table 6: Noise diode correction factors are found for each segment of data using the brightness temperature histograms method. The average correction factor is then applied prior to validation.

MM-2A Channel	Segment 1 (K)	Segment 2 (K)	Segment 3 (K)	Segment 4 (K)	Segment 5 (K)	Segment 6 (K)	Average Correction (K)
1	+160	+175	+107	+141	+162	+109	+142
2	-3.8	-2.9	-3	-3.6	-3.4	-2.8	-3.3
3	-6.0	-4.9	-1.4	-2.6	-0.2	-3.8	-3.1
4	-4.7	-2.8	-2.8	-4.0	-1.8	-4.4	-3.4
5	-9.5	-9.1	-14.7	-12.8	-15.7	-11.2	-12.2
6	-10.7	-9.4	-22.0	-18.7	-22.2	-15.0	-16.3
7	+7.6	-11.2	+0.9	-10.4	+0.2	-1.0	-2.3
8	-119	-85	-115	-110	-136	-115	-113
9	+5.7	+4.0	+0.6	+3.7	-2.2	-2.7	+1.5

V. Results

In this section, we show the calibration results using brightness temperature histograms between MicroMAS-2A and MWHS-2 data segments, and we also provide the validation results using single differences between MicroMAS-2A and CRTM with ERA5 inputs.

A. Calibration Correction Results

In Table 6 we show the noise diode correction factors that are found for each segment of data using the brightness temperature histograms method. The varying correction factor results for each data segment are likely due to two main factors: 1) the simplified noise diode scheme used in this analysis that does not take into account instrument temperature and 2) the lack of adequate noise diode TVAC testing for MicroMAS-2A. Both of these factors will the addressed for the future mission TROPICS.

We then find the average calibration correction and apply it to each segment of MicroMAS-2A data prior to radiance validation. Table 7 shows the prelaunch noise diode calibration, the average calibration correction, and the final noise diode temperature after correction.

B. Validation Results

We next use the single difference technique to compare CRTM/ERA5 simulated brightness temperatures to the MicroMAS-2A points selected for each data segment. Table 8 shows the average single difference and standard deviation for the 41 selected data segment points.

Channels 1-5 show average single differences between 0.38 K to 2.2 K. Channels 7-9, the water vapor channels, have average single differences between 2.2 and 3.2 K. Channel 6 has an average single difference of approximately 8.8 K; the discrepancy with Channel 6 is most likely due to the multiple peaks shown in the Channel 6 as-measured SRF weighting functions, and the subsequent weighting function mismatch with MWHS-2 channels. The standard deviations of all channels is under 2.6 K, with the exception of Channels 1 and 7. Channel 1 is likely impacted by surface effects, and further investigation is needed to explain the relatively large standard deviation in the Channel 7 comparisons, which could potentially be attributed to errors in the sensor transfer function assumptions.

Table 7: Updated noise diode temperatures are found by applying average calibration corrections from data segments 1-6. Calibration corrections are determined by using histogram matchups between MicroMAS-2A and MWHS-2.

MM-2A Channel	Pre-launch (K)	Average Calibration Correction (K) (Seg 1-6)	After correction (K)
1	1945	+142	2087
2	226	-3.3	222.7
3	223	-3.1	219.9
4	206	-3.4	202.6
5	188	-12.2	175.8
6	205	-16.3	188.7
7	309	-2.3	306.7
8	827	-113	714.0
9	499	+1.5	500.5

Table 8: Average single difference and standard deviation between MicroMAS-2A and CRTM over the 41 selected data points.

MM-2A Channel	Average Single Difference (K)	Standard Deviation (K)
1	-1.15	5.71
2	0.62	1.22
3	2.20	1.10
4	-1.87	0.74
5	-0.38	0.66
6	-8.81	0.99
7	-3.10	5.67
8	2.24	2.60
9	-2.80	1.83

Table 9: Single differences are also calculated using differing subsets of 30 points from the total 41 points in order to check for robustness.

MM-2A Chan-nel	Average Single Differences (all 41 points)	Average Single Differences (Points 1-30)	Average Single Differences (Points 5-35)	Average Single Differences (Points 10-40)
1	-1.15	-5.52	-1.31	4.25
2	0.62	0.08	0.54	1.37
3	2.20	1.93	1.99	2.45
4	-1.87	-2.12	-2.16	-1.88
5	-0.38	0.08	0.26	0.29
6	-8.81	-8.39	-8.06	-8.02
7	-3.10	-2.88	-2.67	-1.52
8	2.24	3.33	2.98	2.52
9	-2.80	-3.64	-3.06	-1.51

To check for robustness, average single differences were then recomputed using various realizations of 30 of the total 41points. The results are shown below in Table 9. The average single differences for Channels 3-6 are within 0.6 K of each other, while the average single differences of Channels 2 and 7-9 are within 1.6 K of each other. Channel 1 shows the most variation in single differences (within 4.5 K), and is likely impacted by surface effects. With the exception of Channel 1, single differences appear to hold up to subset selection.

VI. Conclusion

We have shown initial calibration and radiance validation results for MicroMAS-2A data segments 1-6. Comparisons between MicroMAS-2A and MWHS-2 brightness temperature histograms are used to provide on-orbit noise diode correction factors. Radiance validation of the six MicroMAS-2A data segments is performed using CRTM with inputs from ERA5. It is particularly encouraging that the intercomparison of MicroMAS-2A to CRTM over a limited dataset shows biases of less than 2.2 K for Channels 1-5, and further improvements are expected for the forthcoming NASA TROPICS mission. Although the MicroMAS-2A mission was only able to downlink limited data, the data collected demonstrates the promise of using miniaturized microwave radiometers for low-cost weather monitoring platforms.

Future work will continue improving these results. We are analyzing methods of developing a more sophisticated noise diode correction scheme that will take into account instrument temperature, as well as lessons learned from TROPICS TVAC testing. There is a desire to launch the TROPICS Engineering Model (EM) in 2020, and our methods and models developed in this work could be used for the radiance validation of the TROPICS EM in the near future. We expect that having a larger number of datasets will allow us to further trend and improve the calibration and validation of the CubeSat data. Lessons learned from MicroMAS-2A calibration and validation will be applied to the future constellation TROPICS.

References

[1] ECMWF. ERA5. \https://www.ecmwf.int/en/forecasts/datasets/archive-datasets/reanalysis-datasets/era5.

[2] Joint Center for Satellite Data Assimilation. Community radiative transfer model. \https://www.jcsda.noaa.gov/projects_crtm.php.

[3] Marinan, et al. “Analysis of the Microsized Microwave Atmospheric Satellite (MicroMAS) Communications Anomaly,” *Journal of Small Satellites*, vol. 7, No. 1, pp. 683-689, 2018.

[4] Blackwell W. J., Braun S., Bennartz R., Velden C., DeMaria M., Atlas R., Dunion J., Marks F., Rogers R., Annane B., and Leslie R. V. An overview of the TROPICS NASA earth venture mission. Quarterly Journal of the Royal Meteorological Society, 0(ja).

[5] W. J. Blackwell, "Design and Performance of the Tropics Radiometer Components," *IGARSS 2018 - 2018 IEEE International Geoscience and Remote Sensing Symposium*, Valencia, 2018, pp. 1024-1027. doi: 10.1109/IGARSS.

[6] A. Crews, W. Blackwell, R. V. Leslie, M. Grant, K. Cahoy. Solar and Lunar Calibration for Miniaturized Microwave Radiometers. Proceedings of IEEE Aerospace Conference, 2019.

[7] W. J. Blackwell *et al*., "Hyperspectral Microwave Atmospheric Sounding," in *IEEE Transactions on Geoscience and Remote Sensing*, vol. 49, no. 1, pp. 128-142, Jan. 2011. doi: 10.1109/TGRS.2010.2052260

[8] W. Blackwell, J. Pereira, “New Small Satellite Capabilities for Microwave Atmospheric Remote Sensing: The Earth observing Nanosatellite-Microwave (EON-MW)”, in CalPoly Workshop, San Luis Obispo, 2015.

[9] W. Blackwell et al. Micromas: A first step towards a nanosatellite constellation for global storm observation. In AIAA/USU Conference on Small Satellites, 27th Annual CubeSat Developers’ Workshop, 2013

[10] S. T. Brown, S. Desai, W. Lu, and A. Tanner. On the long term stability of microwave radiometers using noise diodes for calibration.

IEEE Transactions on Geoscience and Remote Sensing, 45(7):1908–1920, May 2007.

[11] D. W. Draper, D. A. Newell, D. S. McKague, and J. R. Piepmeier. Assessing Calibration Stability using the Global Precipitation Measurement (GPM) Microwave Imager (GMI) noise diodes. *IEEE Journal of Selected Topics in Applied Earth Observations and Remote Sensing*, 8(9): 4239-4247, Sept 2015.

[12] D. Draper and D. Newell, "Global Precipitation Measurement (GPM) Microwave Imager (GMI) After Four Years On-Orbit," 2018 IEEE 15th Specialist Meeting on Microwave Radiometry and Remote Sensing of the Environment (MicroRad), Cambridge, MA, 2018, pp. 1-4. doi: 10.1109/MICRORAD.2018.8430702

[13] Quadrino, Meghan K. (2014). *Testing the Attitude Determination and Control of a CubeSat with Hardware-in-the-Loop*. Master's thesis, Massachusetts Institute of Technology, Cambridge, MA.

[14] Crassidis, J. L., & Junkins, J. L.(2004). 7.2: Attitude Estimation. In Optimal Estimation of Dynamic Systems (pp. 419-433). Boca Raton,FL: Chapman & Hall/CRC.

[15] Kleespies, T. (n.d.). *A Discussion of Radiative Transfer Models*. Retrieved from https://www.jcsda.noaa.gov/documents/meetings/.../Kleespies07301030.ppt.

[16] Bormann, N. and Geer, A. and English, S. "Evaluation and comparisons of FASTEM versions 2 to 5". Retrieved from https://cimss.ssec.wisc.edu/itwg/itsc/itsc18/program/files/links/8.07_Bormann_pa.pdf.

[17] Liu, Quanhua & Weng, Fuzhong & English, Stephen. (2011). An Improved Fast Microwave Water Emissivity Model. Geoscience and Remote Sensing, IEEE Transactions on. 49. 1238 - 1250. 10.1109/TGRS.2010.2064779.

[18] CDAAC: COSMIC Data Analysis and Archive Center. https://cdaac-www.cosmic.ucar.edu.

[19] GRUAN. GCOS reference upper-air network. \https://www.gruan.org//.

[20] Copernicus. ERA5 hourly data on single levels from 1979 to present. https://cds.climate.copernicus.eu/cdsapp#!/dataset/reanalysis-era5-single-levels?tab=overview.

[21] H. Lawrence, N. Bormann, Q. Lu, A. Geer, and S. English. An Evaluation of FY-3C MWHS-2 at ECMWF. EUMETSAT/ECMWF Fellowship Programme Research Report No. 37, June 2015.

[22] S. Zhang *et al*., "Design of the second generation microwave humidity sounder (MWHS-II) for Chinese meteorological satellite FY-3," *2012 IEEE International Geoscience and Remote Sensing Symposium*, Munich, 2012, pp. 4672-4675. doi: https://doi.org/10.1109/IGARSS.2012.6350423

[23] S. Biswas, S. Farrar, K. Gopalan, A. Santos-Garcia, W. Jones, S. Bilanow, "Intercalibration of Microwave Radiometer Brightness Temperatures for the Global Precipitation Measurement Mission," *IEEE Transactions on Geoscience and Remote Sensing*, vol. 51, no. 3, pp. 1465-1477, 2013.

[24] C. Ruf. Detection of Calibration Drifts in Spaceborne Microwave Radiometers using a Vicarious Cold Reference. IEEE Transactions on Geoscience and Remote Sensing, 38(1):44-52, Jan 2000.

BIOGRAPHY

Angela Crews received a B.S. in aerospace engineering from the United States Naval Academy, Annapolis, MD in 2004. She received dual M.S. degrees in aeronautical engineering and astronautical engineering from the Air Force Institute of Technology, Dayton, OH in 2012. From 2004 to 2015, she served in the United States Marine Corps (USMC) as an EA-6B Electronic Countermeasures Officer (ECMO) and as a Space Operations Officer. Crews received a Ph.D in 2019 from MIT. While at MIT, she was a student in MIT's STAR Lab in the AeroAstro Department. Her research was focused on calibration and validation for miniaturized microwave radiometers. Dr. Crews is currently a Space Subject Matter Expert (SME) for Mantech International in support of the Marine Corps Warfighting Laboratory.

Kerri Cahoy is an Associate Professor of Aeronautics and Astronautics at MIT and leads the Space Telecommunications, Astronomy, and Radiation (STAR) Laboratory. Cahoy received a B.S. (2000) in Electrical Engineering from Cornell University, and M.S. (2002) and Ph.D. (2008) in Electrical Engineering from Stanford University. Dr. Cahoy previously worked at Space Systems Loral, as a postdoctoral fellow at NASA Ames, and currently leads nanosatellite atmospheric sensing, optical communications, and exoplanet technology demonstration missions.

William J. Blackwell (M'02–SM'07–F'19) received the Sc.D. degree in electrical engineering and computer science from MIT in 2002. He is now the Associate Leader of the Applied Space Systems Group at MIT Lincoln Laboratory. His research involves environmental monitoring using ground, air, and space-based sensors, and he now serves as the Principal Investigator for the NASA TROPICS Earth Venture mission.

R. Vincent Leslie received the B.S. degree from Boston University, Boston, MA, USA, and the M.S. and Ph.D. degrees from Massachusetts Institute of Technology (MIT), Cambridge, MA, in 1998, 2000, and 2004, respectively, all in electrical engineering.

He was a Graduate Research Assistant with the Remote Sensing and Estimation Group, Research Laboratory of Electronics, MIT, specializing in passive microwave radiometry. He is a member of the Technical Staff in the Applied Space Systems Group at MIT Lincoln Laboratory and currently the TROPICS Instrument Scientist.

Michael Grant received the M.E. and Ph.D. degrees in Electrical and Computer Engineering from the University of Virginia. Since 1987 he has been with the NASA-Langley Research Center, in Hampton, Virginia, working in the areas of spaceflight electronics design, systems engineering, and signal processing on a number of Space Shuttle, aircraft- and satellite-based atmospheric science projects. He is currently the Chief Engineer covering the TROPICS project for the Langley Technical Authority. Dr. Grant's research interests include earth remote sensing, image processing, and pattern classification.

Idahosa A. Osaretin (M'10–SM'19) received the B.S. degree in electrical and computer engineering in 2006, the M.S. degree in electrical engineering in 2010, and the Ph.D. degree in electrical engineering in 2011, all from the Ohio State University, Columbus OH. From 2006 to 2011, he was a Research Associate with the ElectroScience Laboratory at the Ohio State University. Since 2011, he has worked at MIT Lincoln Laboratory, Lexington MA, where he is currently a member of the Technical Staff. His current research interests include microwave radiometer design, miniaturization, and analysis; compact reflector antenna design; design of compact and wideband horn feeds; low profile ultra-wide band antenna design and analysis; and electromagnetic wave propagation in complex environments.

Michael DiLiberto received a B.S. degree in electronic engineering technology from Wentworth Institute of Technology, Boston, MA in 2008 and a M.S. degree in electrical engineering from Tufts University, Medford, MA in 2012.

He has worked at MIT Lincoln Laboratory since 2008 and is currently an associate staff member in the Applied Space Systems group.

Adam Milstein. Since 2004, Dr. Adam B. Milstein has been a Member of the Technical Staff at MIT Lincoln Laboratory. Dr. Adam B. Milstein has led and contributed to a wide variety of projects related to electro-optics and remote sensing of the Earth. Recently, he has served as principal investigator of the Computational Reconfigurable Imaging Spectrometer (CRISP), an instrument concept aimed at making multi- and hyperspectral infrared measurements on smaller spacecraft. He is also leading development of neural network algorithms for retrieving vertical profiles of temperature and water vapor from microwave and hyperspectral infrared sounders as part of NASA's Sounder Science Team. His other work has included CubeSat attitude control system development, laser radar signal processing algorithmd development, diffuse optical tomography, and image navigation and registration for geostationary satellite imagery.

Stephen Leroy is currently a Principal Scientist at Atmospheric and Environmental Research, Inc. He obtained a B.A. in Physics (1988) from Cornell University and a M.Sc. (1990) and Ph.D. (1994) in Planetary Science from the California Institute of Technology. His previous positions were as a Scientist at the NASA Jet Propulsion Laboratory (1994–2004) and as a Project Scientist in Prof. James Anderson's at Harvard University (2004–2017). His research has covered atmospheric internal gravity waves, GNSS radio occultation, nadir spectral infrared sounding, detection and attribution of climate change, and Bayesian information theory applied to remote sensing data types.

Amelia Gagnon is currently a master's student in the Space Telecommunications, Astronomy, and Radiation (STAR) Laboratory at MIT. She received a B.S. in electrical engineering and a B.A. in music in 2015 from the University of North Dakota. In between undergrad and graduate school, Amelia worked at the Johns Hopkins University Applied Physics Laboratory on systems engineering for the Parker Solar Probe and on electrical engineering design relating to the Europa Clipper.